



Quantum chemical pathways for the formation of 2,3,7,8-tetrachloro dibenzo-*p*-dioxin (TCDD) from 2,4,5-trichlorophenol: a mechanistic and thermo-kinetic study

Raghibul Hussain¹ · Sk. Musharaf Ali^{2,3} · Gopal Pugazhenth¹ · Tamal Banerjee¹

Received: 29 March 2024 / Accepted: 30 May 2024 / Published online: 8 June 2024
© The Author(s), under exclusive licence to Springer-Verlag GmbH Germany, part of Springer Nature 2024

Abstract

Context Dioxins, specifically 2,3,7,8-tetrachlorinated dibenzo-*p*-dioxin (TCDD), are highly toxic dioxins known for their severe health impacts and persistent environmental pollutants. This study focuses on understanding the formation pathways of TCDD from its precursor molecule 2,4,5-trichlorophenol (2,4,5-TCP). In our exploration of reaction pathways from 2,4,5-trichlorophenol (TCP), we delve into three reaction mechanisms: free-radical, direct condensation, and anionic. Our findings highlight the significance of the radical mechanism, particularly propagated by H radicals, with a notable increase in dioxin formation around 900 K. These results are consistent with experimental observations indicating an increase in the conversion of trichlorophenol from 600 to 900 K in the non-catalytic gas phase reaction. Thermodynamic parameters (ΔH , ΔS , and ΔG), reaction barriers, and rate constants (k) were calculated across a temperature range of 300–1200 K to support the findings and provide insights into the optimal temperature range for controlling dioxins during the incineration process. **Method** In this study, quantum chemical calculations were conducted using density functional theory (DFT) with the B3LYP functional and the 6–311 + G(d,p) basis set in Gaussian 16 software. Stationary points, including transition states (TS), were confirmed with frequency calculations. Intrinsic reaction coordinate (IRC) calculations ensured minimum energy paths between TS and products, visualized in GaussView 6.0 Program. Single-point energy calculations utilized a more precise basis set, 6–311 + G(3df,2p), for enhanced energy accuracy, incorporating zero-point vibrational energy (ZPE) and other energy corrections. These calculations were repeated over a temperature range of 298.15–1200 K at 1 atm pressure. Finally, rate constant (k) expressions associated with TCDD formation were determined using transition state theory (TST).

Keywords Chlorophenol · Dioxin · Toxicity · DFT · Transition state theory · Reaction pathways

Introduction

Polychlorinated dibenzo-*p*-dioxins (PCDDs) and dibenzofurans (PCDFs), broadly known as dioxins (PCDD/Fs), are the harmful pollutants that have a direct impact on the

human health, wildlife, and the environment, due to their chronic toxicity [1, 2]. These compounds are recognized as persistent environmental pollutants, resisting easy biodegradation or metabolism because of their high thermal stability and low volatility. Their persistence in the environment raises concerns about potential long-term ecological and human health consequences. Dioxins (PCDD/Fs) are composed of a triple-ring structure, with two benzene rings linked by a third oxygenated ring (Fig. 1). However, different forms of dioxins and their toxicity heavily depend on the number and position of the chlorine atom attached to the triple-ring structure. Among 75 isomers of toxic PCDDs, 2,3,7,8-tetrachlorinated dibenzo-*p*-dioxin (TCDD) is considered as the most toxic dioxin ever known. It is 4×10^6 times more deadlier than octa-chloro substituted dioxin (octa chlorinated dibenzo-*p*-dioxin, OCDD) for the house mice [3]. TCDD is soluble in fat tissues and, therefore, food products

✉ Sk. Musharaf Ali
musharaf@barc.gov.in

✉ Tamal Banerjee
tamalb@iitg.ac.in

¹ Department of Chemical Engineering, Indian Institute of Technology, Guwahati, Assam 781039, India

² Chemical Engineering Division, Bhabha Atomic Research Centre Mumbai, Mumbai, India

³ Homi Bhabha National Institute, Anushaktinagar, Mumbai, India

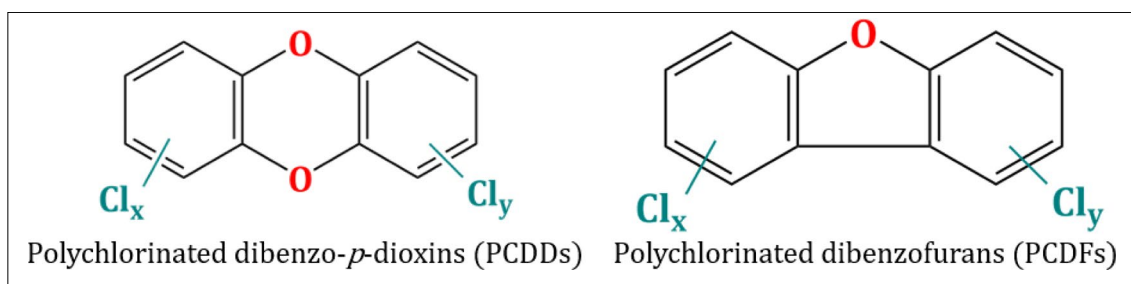


Fig. 1 Generalized chemical formula for dioxins, where Cl_x and Cl_y represent the varying degrees of chlorination in the compounds

like meat, eggs, fish, and dairy products are the potential carrier of this pollutant and ultimately accumulated in human body. This can be inferred from the fact that the average half-life of TCDD in a 75 kg adult man is about 7.6 years that are enough to cause serious health issues including cancer, birth defects, and severe psychological problems [4, 5]. Children and infants are identified as the most sensitive population group in this regard. Also, its effect can last for many generations, the best example is the Vietnam war, during which a toxic herbicide “Agent Orange” was used that contained a significant amount of 2,3,7,8-TCDD [6]. Even after many decades, exposure to the herbicide continues to cause health issues, including cancers, birth defects, and other complications, affecting both veterans and civilians.

Dioxins are unintentionally produced by-products that are mostly emitted by the incomplete combustion and incineration process of municipal solid waste (MSW) [7–9]. However, many anthropogenic activities, such as the chemical industry—handling chlorinated organic compounds, sewage sludge, and hazardous nuclear waste are also equally contributing for its emission [10]. Based on a study conducted by Wang and their co-authors [11], Asian countries almost contribute 50% of the total global dioxins (PCDD/Fs) release. Therefore, it has been a matter of great concern among the scientific communities to control the emission of these toxicants. At the same time, the detailed study of the reaction mechanisms leading to the formation of dioxins contributes to sustainable engineering by providing a foundation for developing strategies to control, inhibit, or remediate their production. Several texts elaborate the formation pathways of dioxin-like compounds [12], notably through the de-novo and the precursor process [13–16]. The precursor process involves the conversion of organic precursors like chlorophenols (CPs), chlorobenzenes (CBs), and polycyclic aromatic hydrocarbons (PAHs), which tends to yield higher amounts of dioxins compared to the more intricate de-novo formation [17, 18]. Dioxin formation is often catalyzed by metals or metal oxides present on fly ash surfaces [19], typically occurring at temperatures ranging from 550 to 750 K. However, in the absence of catalysts, these reactions can take place at higher temperature. A non-catalytic gas-phase study conducted by Lujik et al. [20] found that the

conversion of trichlorophenols into polychlorinated dibenzo-*p*-dioxins (PCDDs) experiences an increase in yield between 600 and 900 K. Okamoto and Tomonari [21] conducted a study in which they analyzed the twelve potential pathways for the formation of PCDDs from 2,4,5-trichlorophenol (TCP) through quantum chemical calculations. They found that radical pathways can be dominated over condensation pathways, if O–H bond of 2,4,5-TCP is broken by simply absorbing ultraviolet (UV) light or other radicals. However, the energy pathways reported by them overlook the inclusion of temperature and entropy effects, which cannot provide information about the spontaneity of reactions. Farajian et al. [22] found in their study that the rate-limiting step in dioxin formation is the closure of the central ring. According to their findings, two chlorophenols lose their hydrogen atoms connected to the oxygens. Afterward, they share their oxygens, resulting in the formation of a closed ring between two benzene rings. This tricyclic ring formation is a crucial step in the emission of dioxins through the chlorophenol pathways. In contrast, Suárez et al. [23] argued that at elevated temperature, the rate-determining step (RDS) for the entire process is the formation of the initial predioxin due to a high Gibbs energy barrier. However, at lower temperatures, they found that the Gibbs energy barrier for this step is similar to those for its evolution into trichlorodioxin. This contradicts the earlier claim by Farajian et al. [22], who asserted that the rate-limiting step is the closure of the central ring in dioxin formation. However, these studies did not address the thermodynamic aspects of the reaction pathways in detail and the reaction conditions that can be used to suppress the formation of dioxins. In actual combustion processes, PCDD/Fs formation mechanism and its favorable synthesis route are very complicated as they involve a variety of chemical compounds, chemical reactions, and products. Hence, there is a need to thoroughly address the formulation of reaction mechanisms via various pathways for the formation of these pollutants, including their thermodynamic considerations and kinetic behavior, which appears to be lacking in the available literature. The toxic nature of dioxins (PCDD/Fs) limits experimental studies and restricts the availability of sufficient data to describe the reaction scheme of their formation. Furthermore, PCDD/Fs are emitted in trace quantities, sometimes

as low as parts per billion (ppb), which also adds to the difficulty of analyzing the rate of dioxin formation at such a very low concentration. Therefore, computational approaches that can provide insights into the formation mechanisms of PCDD/Fs, along with their reaction kinetics, even in the absence of experimental data, are essential for predicting their favorable pathways.

In this study, we investigate the non-catalytic precursor process in the gas phase using density functional theory (DFT) calculations. Our goal is to predict the formation pathways of the highly toxic dioxin, 2,3,7,8-tetrachlorinated dibenzo-*p*-dioxin (TCDD) from 2,4,5-trichlorophenol (2,4,5-TCP). We have selected 2,4,5-TCP for our study due to two main reasons. First, it has a salient chlorine atom in the ortho-position of the hydroxyl group (-OH). Second, it has the minimum required number of chlorine atoms to form the TCDD ring. These qualities make 2,4,5-TCP an ideal choice for our study to investigate the formation pathways for TCDD. In the earlier part of the reaction, two molecules of 2,4,5-TCP combine to form a dimeric compound, which is referred to as predioxin. The structure primarily consists of two benzene rings connected by an oxygen atom. There is a hydroxyl group situated in the ortho position of one benzene ring relative to the C–O–C bond, with chlorine atoms are attached to specific positions on each of the benzene rings. This study includes three most common formation pathways of 2,3,7,8-TCDD from 2,4,5-TCP, viz., (i) pathways via free-radical mechanism, (ii) pathways via direct condensation, and (iii) pathways via anionic mechanism. The initial mechanism of these pathways is different; however, they end with the formation of predioxin. Later on, the condensation of predioxin produces TCDD. In a similar study, Okamoto and Tomonari [21] found that the desorption of HCl is easier, requiring 1.5 to 2 times less barrier than H₂ desorption during the formation of dioxin from 2,4,5-TCP. Therefore, we have exclusively focused on the former condition in our study. Furthermore, to study the spontaneity of the proposed paths, thermodynamic analysis is done by considering the values of ΔG , ΔS , and ΔH at different temperatures. Thermodynamic analysis, reaction barrier, and the rate constant associated with the favorable path not only provides insight into the reaction mechanism but can also be helpful to make strategy to suppress the formation of dioxins. Additionally, these insights can aid in the design of reactors and incinerators, ensuring they operate within a suitable temperature range to effectively control dioxin emissions.

Computational details

In the present work, quantum chemical calculations were performed using the density functional theory (DFT), implemented in the Gaussian 16 series of programs [24] with the

B3LYP functional [25, 26] along with split valence basis set [27] 6–311 + +G(d,p). The structural optimization of the reactants, products, intermediates, and transition states (TS) was performed at the B3LYP/6–311 + +G(d,p) level of theory to study the formation pathways of TCDD from 2,4,5-TCP. The potential energy surface (PES) scan was performed to locate the stationary points. The nature of each stationary point and their vibrational modes has been confirmed using frequency calculations, and the same were examined with the help of GaussView 6.0 Program [28]. The stationary point at minima has all real frequencies, while the transition state (TS), also known as the first-order saddle point, has only one imaginary frequency corresponding to their optimized electronic structure. Furthermore, the intrinsic reaction coordinate (IRC) [29, 30] calculations were carried out at the same level of theory to make sure that each TS connected its reactions and products via a minimum energy paths (MEP) on the potential energy surface. The optimized geometries were then utilized for single point energy calculations using a more precise basis set 6–311 + +G(3df,2p) to enhance the energy accuracy. However, highly accurate ab-initio methods like CCSD(T) (coupled cluster with singles, doubles, and optional triples terms) are not considered here for single-point energy calculations due to the high computational demands for our systems [31]. In contrast, the B3LYP method offers a balanced approach with sufficient accuracy and moderate computational effort at the 6–311 + +G(3df,2p) basis set, making it suitable for studying the mechanisms and kinetics of gas-phase reactions involving PCDD/Fs. The overall quantum chemical calculation can be denoted as B3LYP/6–311 + +G(3df,2p) // B3LYP/6–311 + +G(d,p). However, for the open shell species having unpaired electrons, a restricted open shell energy calculation (ROB3LYP/6–311 + +G(3df,2p)) was carried out to avoid the spin contamination [32]. The harmonic vibrational frequency calculations were performed on the B3LYP/6–311 + +G(d,p) optimized geometries, at the same level of theory, for each reaction species to obtain their zero-point vibrational energy (ZPVE or ZPE) correction, thermal correction to energy, enthalpy, and Gibbs free energy. The ZPE, thermal corrections, and the effect of entropy were added to the final energy calculation to evaluate the change in Gibbs reaction energy (ΔG) and Gibbs energy barrier height (ΔG^\ddagger) for every elementary reaction. The calculations were repeated over the temperature range of 298.15–1200 K with a constant pressure of 1 atm. Also, the expression for the rate constant (k) associated with the formation of TCDD is calculated from the well-known, transition state theory (TST) [33], given by

$$k(T) = \frac{k_B T}{h} \exp\left(-\frac{\Delta G^\ddagger}{RT}\right) \quad (1)$$

Here, k_B , h , R , and T are Boltzmann constant, Planck constant, ideal gas constant, and the system's temperature in

Kelvin, respectively. The Gibbs energy barrier height (ΔG^\ddagger) is defined as $\Delta G^\ddagger = G(TS) - G(\text{reactant})$, where Gibbs energy (G) [34] is general defined by

$$G = H - TS \quad (2)$$

In Eq. (2), H is enthalpy ($E_o + E_{ZPE} + E_{th} + RT$) [35], where of E_o is electronic energy, E_{ZPE} is zero-point energy, and E_{th} represents the cumulative thermal contribution from vibration, rotation, and translation. On the other hand, S denotes the overall entropy contributed by these same factors, and RT represents the thermal enthalpy at temperature T . In addition, ADF package [36] is used for transition state approximation and the visualization of Gaussian output file to generate a high-quality electronic structure for scientific communication.

Results and discussion

Reaction mechanism: formation pathways to TCDD at ambient condition

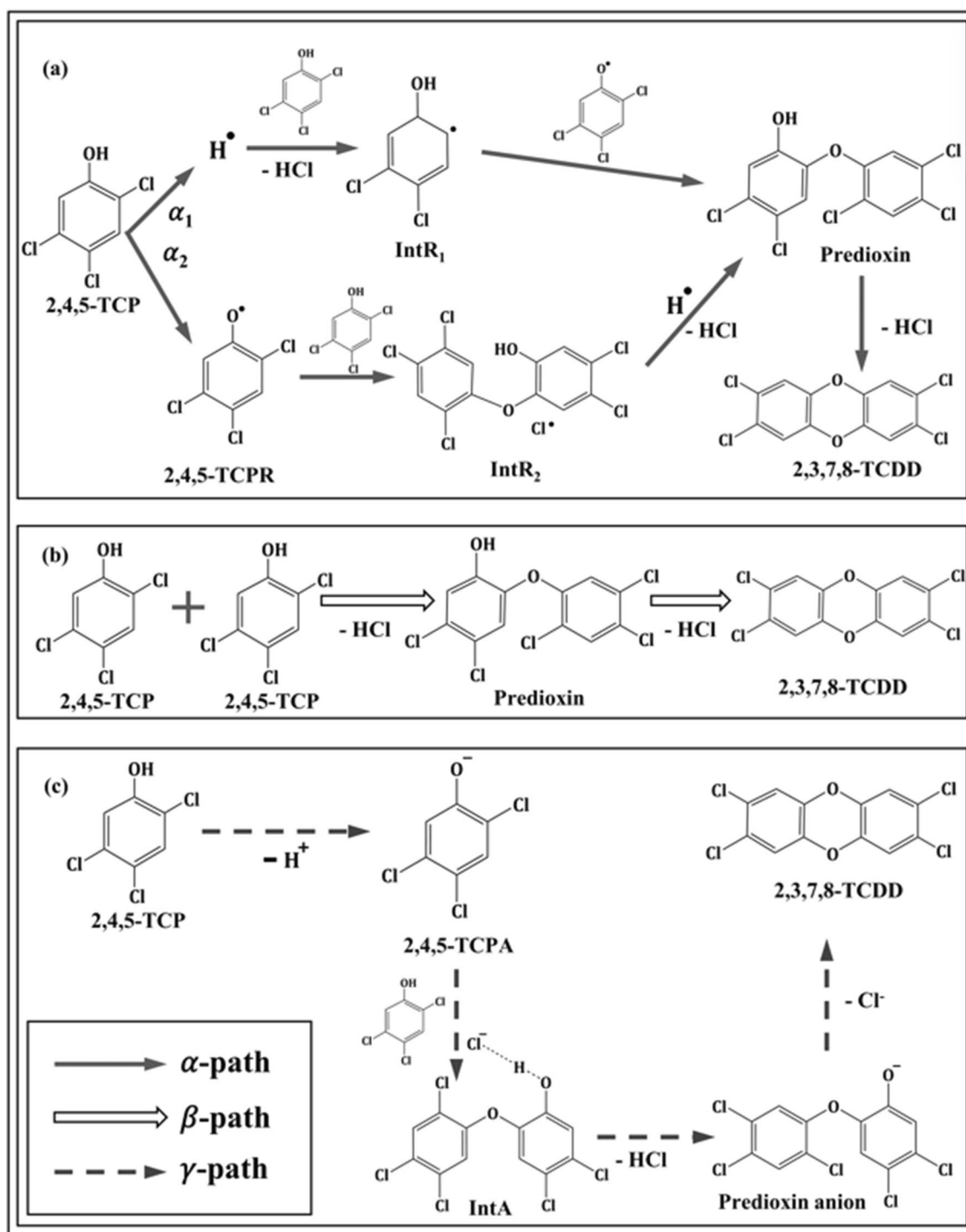
In this work, we proposed three different formation process of 2,3,7,8-tetrachloro dibenzo-p-dioxin (TCDD) in a non-catalytic gas phase environment at 1 atm and at 298.15 K. For all three mechanisms, two molecules of 2,4,5-trichlorophenol (2,4,5-TCP) are allowed to react to form a single molecule of TCDD as a final product. These three pathways are schematically shown in Scheme 1 and were classified into three path type α , β , and γ . The path type α (solid arrows) represents free-radical mechanism, while path type β (bold white arrows) and path type γ (dotted arrows) represent the direct condensation mechanism and the anionic mechanism, respectively. In path type α , the homolytic cleavage of O–H bond of 2,4,5-trichlorophenol produce two radicals, namely, H radical and 2,4,5-trichlorophenoxy radical (2,4,5-TCPR). These two radicals propagate the reaction by reacting with another fresh 2,4,5-TCP to form new intermediate radicals. The newly formed radicals react among themselves to terminate the active radicals and form predioxin (4,5-dichloro-2-(2,4,5-trichlorophenoxy) phenol). On the other hand, path type β also forms the same predioxin molecule by the direct inter molecular condensation of two chlorophenols (2,4,5-TCP). Once predioxin is formed, it undergoes intramolecular condensation, leading to the production of TCDD and the release of an HCl molecule. Besides, the path type γ produces H^+ ion and phenolate anion (2,4,5-TCPA) when OH bond of 2,4,5-TCP breaks heterolytically. Then again, a new molecule of 2,4,5-TCP reacts with this phenolate anion to form an intermediate anion (IntA) followed by predioxin anion. In the end, the peroxide anion closes its dioxin ring by desorbing chloride ion (Cl^-) to form TCDD molecule. In

summary, we categorize the reaction mechanism into two parts: first, the formation of predioxin from 2,4,5-TCP, and second, the dioxin ring-closing mechanism. The formation of initial radicals (H and 2,4,5-TCPR) and anions (H^+ and 2,4,5-TCPA) through O–H bond dissociation demands a significantly higher amount of energy compared to other subsequent reactions, as shown in Table 1. Therefore, we have considered the pathways after the formation of initial reacting species (radicals and anions). For radical pathways, these species can be produced either through exposure to ultraviolet rays or by interaction with other radicals. In the case of anionic pathways, proton abstraction can be facilitated using a suitable strong base. This meticulous approach is crucial for enabling a comparative analysis between radical and anionic pathways. If not considered, the high dissociation energy of the O–H bond, especially in the formation of an anion, could lead to neglecting valuable insights into the reaction mechanism for formation of TCDD from 2,4,5-TCP.

The variation in Gibbs reaction energy (ΔG°) and Gibbs energy barrier height (if applicable, ΔG^\ddagger) for each elementary reaction is outlined in Table 1. The schematic representation of these reactions is presented in Scheme 1.

Formation pathways via free-radical mechanism

When organic molecules undergo bond dissociation, they generate active radicals. In the gaseous phase, 2,4,5-trichlorophenol undergoes homolytic cleavage of its O–H bond without any catalyst. This process results in the formation of both a hydrogen radical and an active radical known as 2,4,5-TCPR. Typically, radicals of this kind can be generated when chlorophenol is exposed to ultraviolet (UV) light; the absorbed energy can be sufficient to break the O–H bond, depending on the wavelength. This initial step is a barrier-less reaction and requires energy of about 75.16 kcal/mol to break the O–H bond. Also, it was observed that the potential curve is attractive along the O–H distance; hence, the transition state is not found during the O–H breaking. After the formation of radicals, the radical reaction pathway further split into two path type, viz., α_1 path type and α_2 path type. In α_1 , the H radical abstracts a Cl atom from the ortho site of the hydroxy group of a fresh 2,4,5-TCP. This leads to the formation of an intermediate radical called IntR₁, which is 13.3 kcal/mol lower in energy than the reactants. This process involves a transition state known as TS_{R2}, which is 15.3 kcal/mol higher in energy than the reactants and results in the release of an HCl molecule (Scheme 1). At this TS, the attacking H atom is 1.62 Å from the salient Cl atom which separates 1.92 Å from the C atom to which it was initially bonded. On the other hand, in path type α_2 , O atom of radical 2,4,5-TCPR attacks the chlorinated C atom in the ortho position of another



Scheme 1 Schematic representation of all reaction species involved in the (a) radical mechanism (solid arrows, top), (b) condensation mechanism (bold white arrows, middle), and (c) anionic mechanism (dotted arrows, bottom) from 2,4,5-trichlorophenol

2,4,5-TCP. This results in the formation of an intermediate molecule called $IntR_2$, which is 24.8 kcal/mol higher in energy compared to the initial reactants. This process proceeds through a transition state known as TS_{R4} , which has a barrier height of 37.6 kcal/mol. At this moment,

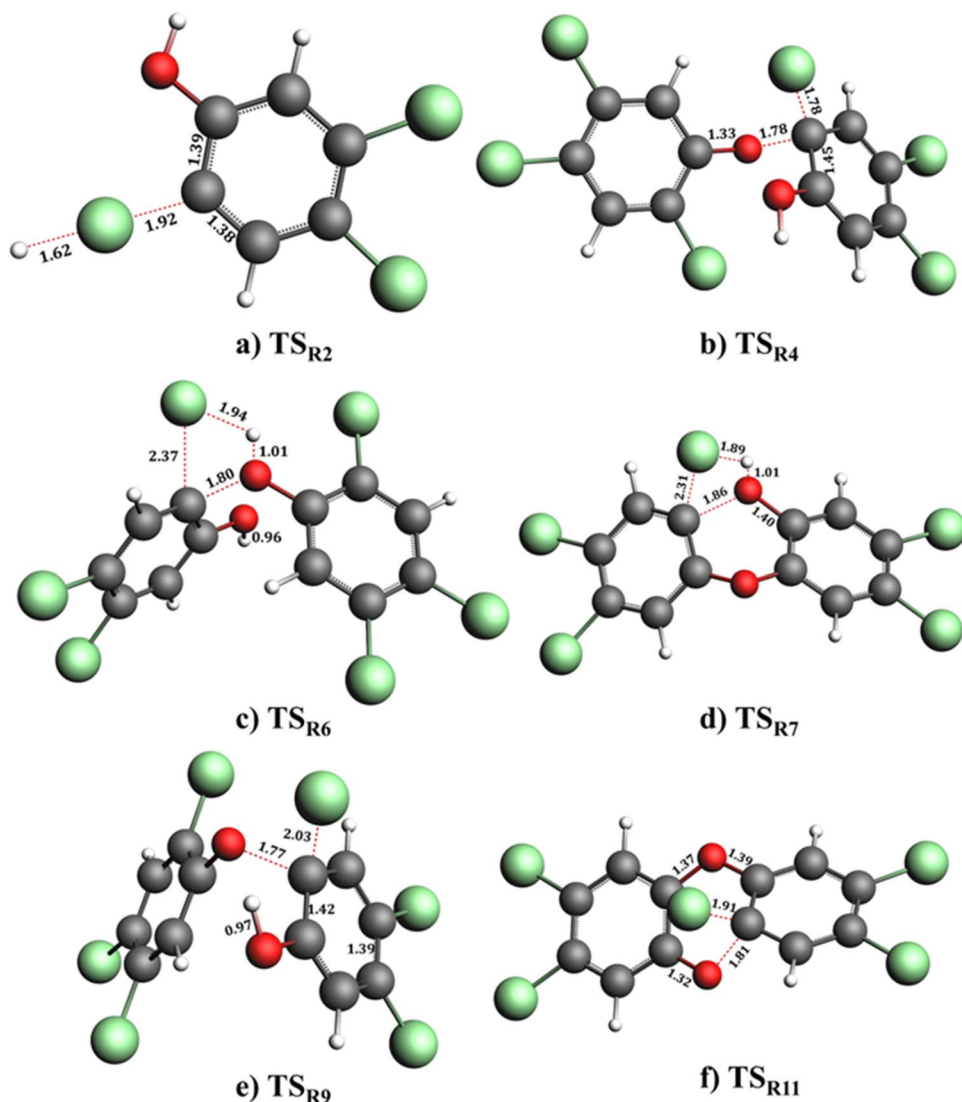
the oxygen atom in the attacking radical, 2,4,5-TCPR, is situated 1.78 Å away from the carbon atom in 2,4,5-TCP. Simultaneously, the chlorine atom of 2,4,5-TCP is also positioned 1.78 Å away from the carbon atom in the ortho position to which it was initially bonded. Figure 2a,

Table 1 The Gibbs reaction energy (ΔG°) and Gibbs activation energy/barrier height (ΔG^\ddagger) (in kcal/mol)^a of the elementary process at 298.15 K and 1 atm

Reaction	Elementary process	ΔG°	ΔG^\ddagger
R1	2,4,5-TCP \rightarrow 2,4,5-TCPR + H	75.16	No ^b
R2	2,4,5-TCP + H \rightarrow IntR ₁ + HCl	-13.28	15.32
R3	IntR ₁ + 2,4,5-TCPR \rightarrow predioxin	-57.26	No
R4	2,4,5-TCP + 2,4,5-TCPR \rightarrow IntR ₂	24.82	37.61
R5	IntR ₂ + H \rightarrow predioxin + HCl	-95.37	No
R6	2 \times 2,4,5-TCP \rightarrow predioxin + HCl	4.62	70.65
R7	predioxin \rightarrow 2,3,7,8-TCDD + HCl	-14.33	59.12
R8	2,4,5-TCP \rightarrow 2,4,5-TCPA + H ⁺	326.33	No
R9	2,4,5-TCP + 2,4,5-TCPA \rightarrow IntA	-13.86	30.38
R10	IntA \rightarrow predioxin anion + HCl	11.54	No
R11	predioxin anion \rightarrow 2,3,7,8-TCDD + Cl ⁻	-0.23	25.19

(a) Energy calculated at B3LYP/6-311++G(3df,2p)//B3LYP/6-311++G(d,p) level of theory. (b) Transition structure is not found for this reaction

Fig. 2 Optimized structures of transition states involve in radical mechanism (a, b), condensation mechanism (c, d), and anionic mechanism (e, f). The key geometrical parameters are given in Å. Red, green, grey, and white spheres represent O, Cl, C, and H atoms, respectively



b illustrates the transition states TS_{R2} and TS_{R4} associated with these radical pathways, and their vibrational frequency is reported in Table S2 (supplementary information). The presence of negative frequency is consistent with transition state theory (TST) for all TS structures shown in Fig. 2. Furthermore, radical–radical coupling between IntR₁ and 2,4,5-TCPR in the path type α_1 leads to the formation of predioxin.

In a similar way, H radical extracts again a Cl atom from IntR₂ and forms predioxin. The formation of predioxin is highly exergonic in nature, releasing 57.26 kcal/mol in path type α_1 and 95.37 kcal/mol in path type α_2 , with no involvement of transition states (TS). Moreover, the predioxin molecule undergoes an intramolecular condensation process in which an HCl molecule is eliminated, resulting in the formation of the highly toxic TCDD molecule. This process will be discussed in detail in the following section as it plays a crucial role in the condensation mechanism.

Formation pathways via inter-molecular condensation mechanism

The β pathway corresponds to an inter-molecular condensation reaction between two molecules of 2,4,5-TCP, followed by the intra-molecular condensation of predioxin. In the earlier part of the reaction, two molecules of 2,4,5-TCP combine to form predioxin. In this process, the elimination of an HCl molecule takes place through a transition state known as TS_{R6} , as depicted in Fig. 2c. It is worth noting that during this transition state, the O–H bond in one 2,4,5-TCP molecule and the C–Cl bond in another 2,4,5-TCP molecule are stretched to 1.01 Å and 2.37 Å, respectively, before breaking from their parent molecules. At the same time, the newly forming bond is separated by distances of 1.94 Å and 1.8 Å for the HCl and predioxin molecules, respectively. In this particular case, the barrier for the removal of HCl is approximately 70.6 kcal/mol, and the energy required to form predioxin is approximately 4.6 kcal/mol. Later on, the predioxin molecule is involved in the intra-molecular condensation reaction to give highly toxic dioxin TCDD, after eliminating another HCl molecule. The transition state for this step, denoted as TS_{R7} , is located 63.7 kcal/mol higher than the reactants. In TS_{R7} , the non-bridged O atom is 1.86 Å away from the attacked C atom, and the salient Cl atom is 2.31 Å apart from the original C atom. Simultaneously, H atom stretched to 1.01 Å from hydroxyl O atom and heading towards salient Cl atom with a separation of 1.89 Å (Fig. 2d).

Formation pathways via anionic mechanism

In the γ pathway, a series of reactions occurs like radical mechanism under non-catalytic and gaseous environment. As mentioned earlier, when the O–H bond in 2,4,5-trichlorophenol (2,4,5-TCP) breaks heterolytically (proton abstraction), it results in the generation of a phenolate anion (2,4,5-TCPA) along with a proton (H^+). Typically, such proton abstraction can be achieved with the help of a strong base. This reaction is highly endergonic, demanding approximately 250 kcal/mol more energy than the formation of the radical associated with breaking the same O–H bond (see Table S3 in supplementary information). Similar to radical mechanism, the transition state is not observed in this reaction during the O–H breaking. In the next step, the nucleophilic substitution reaction is observed when the anionic O atom of 2,4,5-TCPA attacks the chlorinated C atom in the ortho position of 2,4,5-TCP, resulting in the formation of an intermediate anion known as IntA. This reaction involves a transition state called TS_{R9} , which is situated 30.4 kcal/mol above the energy level of the reactants. Meanwhile, the anionic intermediate, denoted as IntA, exhibits a significantly lower energy, approximately –13.9 kcal/mol compared to

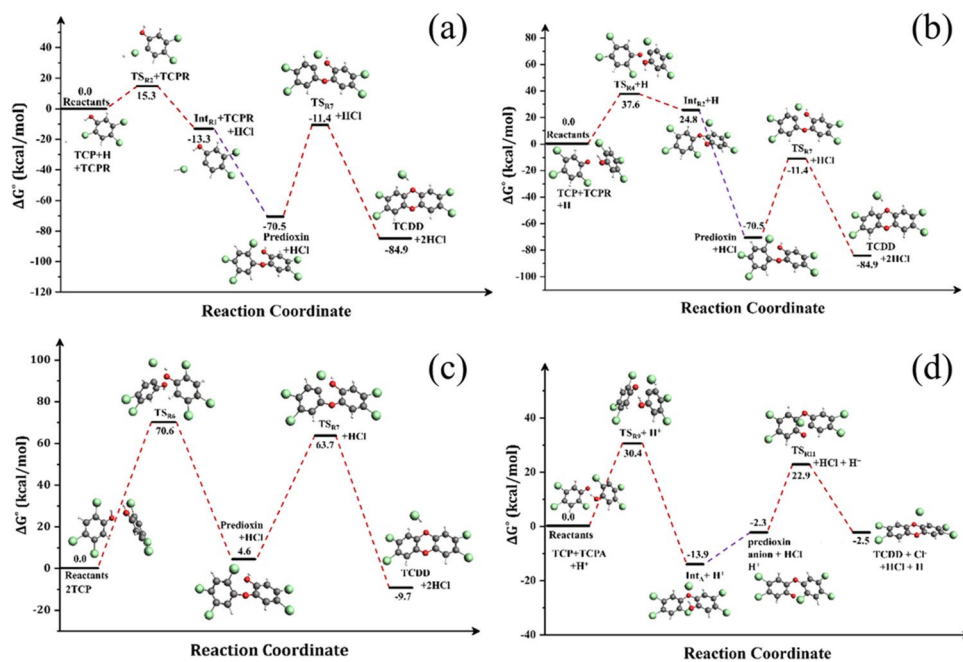
the reactants. In this transition state (TS), the attacking O atom is 1.77 Å away from the attacked C atom, while the prominent Cl atom is positioned 2.03 Å away from the original C atom to which it was initially bonded (refer to Fig. 2e). At IntA, a bridged O atom connects the two phenyl rings, and the significant Cl atom migrates towards the hydroxyl H atom at a distance of 1.94 Å (refer to supplementary information). This intermediate eventually leads to the formation of predioxin-anion, involving the dissociation of O–H bond. It is located 11.54 kcal/mol above the energy of the IntA after eliminating an HCl molecule, and it does not have any transition state (TS). The predioxin anion then proceeds to undergo an intramolecular aromatic nucleophilic substitution reaction. In this step, the non-bridged oxygen atom attacks the chlorinated carbon atom in the ortho position relative to the bridged oxygen atom. This results in the formation of two products: 2,3,7,8-tetrachlorinated dibenzo-p-dioxin and a chloride ion (Cl^-). The transition state (TS) for this reaction is known as TS_{R11} , and it has an activation energy barrier of 25.19 kcal/mol. The reaction releases 0.23 kcal/mol of energy with respect to the predioxin anion. At this transition state, the distance between the attacking oxygen atom and the attacked chlorinated carbon atom is 1.81 Å, and the prominent chlorine atom is separated by 1.91 Å from the carbon atom to which it was originally bonded.

Gibbs free energy profiles

The Gibbs free energy profile provides important insights into chemical reactions, including their thermodynamics, kinetics, and the stability of both reactants and products. Particularly, it offers information about the spontaneity of the reaction at room temperature as it incorporates temperature and entropy effects. Figure 3 displays the variations in ZPE-corrected Gibbs free energy (ΔG°) at 1 atm and 298.15 K for all three proposed mechanisms involving the chemical reactions outlined in Table 1. In Fig. 3, each chemical species represents its presence at a specific moment. The reported Gibbs free energy values consider a series of elementary reactions starting from 2,4,5-TCP to TCDD. However, the Gibbs free energy profiles do not include reactions R1 and R8 in our comparative study. This omission is due to the high bond dissociation energy of the phenolic O–H bond in 2,4,5-TCP, as mentioned earlier, leading to the formation of radicals (or anions).

Consequently, these reactions are not part of the initial reactant shown in the profiles; instead, they are reported separately after the formation of radicals (or anions). The radical mechanism comprises two path types: α_1 , involving reactions R2, R3, and R7; and α_2 , involving reactions R4, R5, and R7 (Figs. 3a and 4b, respectively). In α_1 path type, reaction R2 produces $IntR_1$ and HCl when 2,4,5-TCP reacts with hydrogen. This initial step is thermodynamically

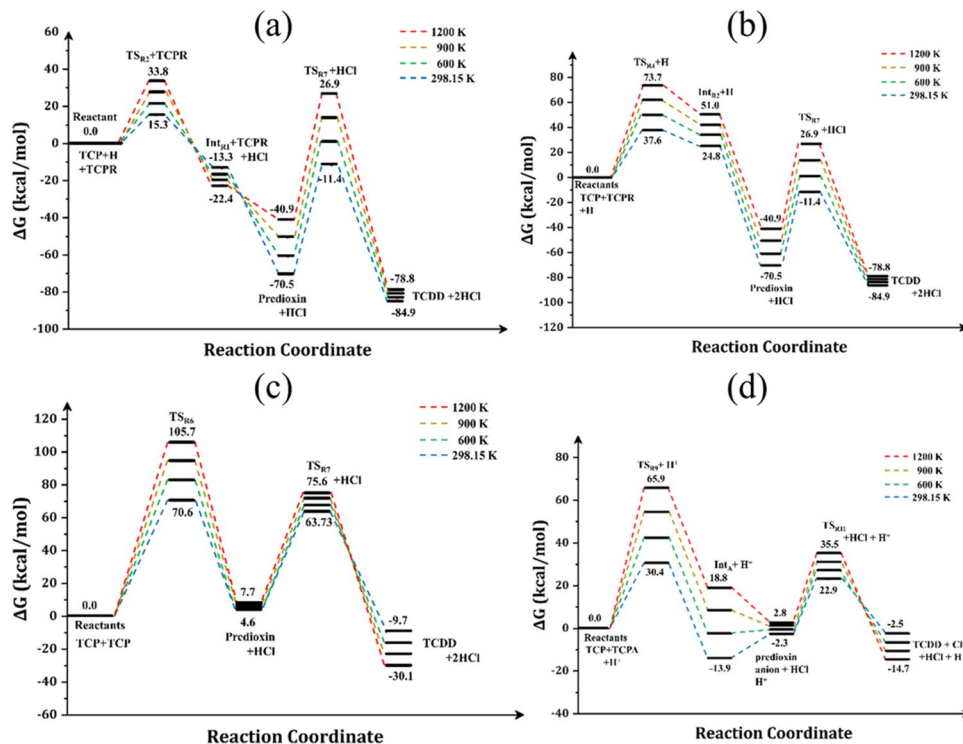
Fig. 3 Gibbs energy profiles for the formation of TCDD from 2,4,5-trichlorophenol at 298.15 K and 1 atm. The profiles illustrate radical pathways (a, b), condensation pathways (c), and anionic pathways (d)



favorable, as indicated by the negative ΔG (-13.3 kcal/mol), and it does have a moderate activation energy barrier ($\Delta G^\ddagger = 15.32$ kcal/mol). In contrast, reaction R4 in α_2 has a positive ΔG ($=24.8$ kcal/mol), indicating an unfavorable thermodynamic change and a relatively higher activation energy barrier ($\Delta G^\ddagger = 37.6$ kcal/mol) than reaction R2. In addition, radical–radical coupling reaction (reaction R3

and R5) contributes to a further reduction in the overall Gibbs free energy (Table 1). In the end, in the final step, both pathways proceed through reaction R7 which involves the transformation of predioxin into 2,3,7,8-TCDD and HCl. The negative ΔG (-14.33 kcal/mol) suggests that it is also a thermodynamically favorable process, with a substantial activation energy barrier ($\Delta G^\ddagger = 59.12$ kcal/mol).

Fig. 4 Gibbs energy profiles as a function of temperature for the formation of TCDD from 2,4,5-trichlorophenol, illustrating radical pathways (a, b), condensation pathways (c), and anionic pathways (d)



As seen in Fig. 3, pathways (a) and (b) are equally favorable as indicated by the overall negative ΔG (-84.9 kcal/mol). Moreover, the Gibbs activation energy barrier of the former pathways is 22.3 kcal/mol lower than that of the latter. Thus, the formation of predioxin, which is the rate-determining step, is more favorable in pathways (a) than pathways (b) and hence the overall pathways (a). Similarly, condensation pathways (Fig. 3c) involve reactions R6 and R7 to produce predioxin and TCDD respectively. In reaction R6, where two molecules of 2,4,5-TCP transform into predioxin and HCl, a high activation energy barrier ($\Delta G^\ddagger = 70.65$ kcal/mol) is found. Despite this, the positive ΔG (4.62 kcal/mol) for this reaction suggests thermodynamic unfavorability. In another reaction R7, predioxin converts into 2,3,7,8-TCDD and HCl. The negative ΔG (-14.33 kcal/mol) denotes thermodynamic favorability, while the substantial ΔG^\ddagger (59.12 kcal/mol) signals a significant activation energy barrier. Hence, the high activation energy barriers (ΔG^\ddagger), especially in R6, may impact the kinetics and overall feasibility of the process at high temperature. Our findings indicate that the formation of predioxin (R6) is the rate-determining step compared to the ring closer mechanism (R7), which is supporting earlier theoretical studies [21, 23]. However, this contradicts an ab-initio molecular dynamic study conducted by Farajian et al. [22], who argued that the closure of the central ring in dioxin formation is the rate-limiting step. The same contradiction is also highlighted in another theoretical study by Suárez et al. [23]. Moreover, the anionic pathways (Fig. 3d) involve reactions R9, R10, and R11 to produce IntA, predioxin-anion, and TCDD, respectively, as a major product. In the first stage, the reaction between 2,4,5-TCP and 2,4,5-TCPA results in the formation of IntA, accompanied by a moderate activation barrier of 30.4 kcal/mol. This reaction is exergonic in nature, as indicated by a negative change in Gibbs free energy ($\Delta G = -13.9$ kcal/mol), signifying its thermodynamic favorability. However, the transformation of IntA into predioxin anion and HCl molecule demands a moderate energy change ($\Delta G = 11.54$ kcal/mol) for the reaction R10. In the subsequent reaction, predioxin anion changes

into 2,3,7,8-TCDD and Cl^- , with a slightly negative ΔG (-0.23 kcal/mol) but a relatively high activation energy barrier ($\Delta G^\ddagger = 25.19$ kcal/mol). Despite this, anionic pathways also appear to be thermodynamically favorable at ambient condition with overall negative ΔG (-2.5 kcal/mol).

Effect of temperature on reaction pathways

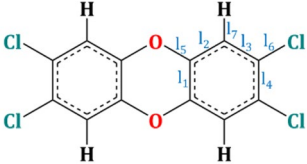
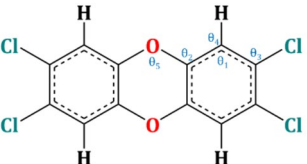
At high temperatures, the Gibbs energy change influences the reaction pathways and their kinetics, providing insights into the overall feasibility of the process. To calculate the rate constant at different temperatures, we identified the rate-determining step (slowest step) for all pathways. It is evident that the first step is clearly the rate-determining one, as discussed earlier, rather than the step corresponding to the formation of the tricyclic ring.

The rate constants, calculated using TST (Eq. 1), are shown in Table 2 for temperatures of 298.15 K, 600 K, 900 K, and 1200 K. Additionally, the ZPE-corrected Gibbs energy changes corresponding to the proposed reaction pathways at these temperatures are shown in Fig. 4. We observed that on increasing temperature, the overall Gibbs energy of the reaction becomes more negative, indicating a more spontaneous and energetically favorable reaction. Also, our findings indicate an increase in the Gibbs energy barrier as the temperature rises, from 298.15 K (15.3 kcal/mol) to 1200 K (33.8 kcal/mol), particularly in the thermodynamically favorable pathway, α_1 . However, this elevation in the barrier is compensated by the temperature increase, leading to a subsequent rise in the rate constant for the formation of 2,3,7,8-TCDD. A similar trend is observed for all other pathways, which is consistent with the transition state theory. At low temperature ($T < 600$ K), a significant rise in rate constant is observed compared to the high-temperature condition ($T > 600$ K) as illustrated in Table 2. Specially, for the radical pathway propagated by H radical (pathway- α_1), the rate constant undergoes a substantial increase of four orders of magnitude, rising from $3.62 \times 10^1 \text{ s}^{-1}$ at 298.15 K to $1.75 \times 10^5 \text{ s}^{-1}$ at 600 K. Subsequently, it undergoes a moderate increase of about two orders of magnitude, reaching $1.77 \times 10^7 \text{ s}^{-1}$ at 1200 K. These

Table 2 Overall change in Gibbs free energy (ΔG , kcal/mol), reaction barrier (ΔG^\ddagger , kcal/mol), and corresponding rate constant (k , sec^{-1}) at different temperatures

Reaction pathways	298.15 K			600 K		
	ΔG^\ddagger	ΔG	k	ΔG^\ddagger	ΔG	k
Pathway- α_1	15.33	-84.88	3.62×10^1	21.55	-83.23	1.76×10^5
Pathway- α_2	37.61	-84.88	1.67×10^{-15}	49.94	-83.23	8.08×10^{-6}
Pathway- β	70.65	-9.72	1.01×10^{-39}	82.72	-16.54	9.25×10^{-18}
Pathway- γ	30.38	-2.55	3.32×10^{-10}	42.54	-6.63	3.98×10^{-3}
	900 K			1200 K		
Pathway- α_1	27.61	-80.99	3.70×10^6	33.76	-78.77	1.77×10^7
Pathway- α_2	62.03	-80.99	1.62×10^{-2}	73.74	-78.77	9.27×10^{-1}
Pathway- β	94.33	-23.24	2.32×10^{-10}	105.70	-30.12	1.40×10^{-6}
Pathway- γ	54.34	-10.68	1.19	65.92	-14.73	24.6

Table 3 Comparison of calculated molecular geometries (in angstroms or degrees) at B3LYP/6-311++G(d,p) level of theory with the X-ray diffraction experimental values [37]

Bond Length (BL)				
Optimized Structure of TCDD (B3LYP/6-311++G(d,p))	BL/BA	Computational Data	Experimental Data	Deviation (%)
	l_1	1.396	1.387	0.65
	l_2	1.385	1.377	0.58
	l_3	1.394	1.384	0.72
	l_4	1.397	1.385	0.87
	l_5	1.378	1.379	-0.07
	l_6	1.744	1.745	-0.06
	l_7	1.082	1.01	7.13
Bond Angle (BA)				
	θ_1	120.2	121	-0.66
	θ_2	118.1	117.6	0.43
	θ_3	118.5	118.9	-0.34
	θ_4	119.3	119	0.25
	θ_5	116.2	115.7	0.43

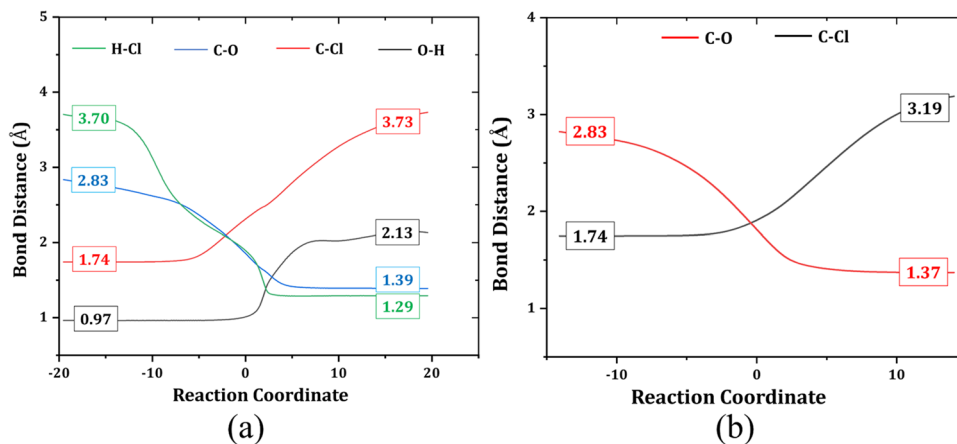
findings reveal that formation of TCDD from 2,4,5-TCP is more prominent at lower temperature (298.15–600 K). However, for another radical pathway (α_2), TST predicts a very low rate constant due to their large energy barrier compared to the pathway- α_2 . In contrast, the condensation pathway (β) has a very high activation energy; as a result, even at elevated temperatures, the fraction of molecules with enough energy to surpass this barrier is still quite low. A very low rate constant indicates that the reaction is not likely to occur at a significant rate under these conditions. The rate constant for anionic pathway (γ) varies from $3.32 \times 10^{-10} \text{ s}^{-1}$ (298.15 K) to 24.6 s^{-1} (1200 K), indicating the

fact that the reaction is very slow at the beginning. Conversely, at higher temperature, reaction rate is getting increased. Therefore, we can conclude that the anionic pathway can also contribute to the formation of TCDD from 2,4,5-TCP at elevated temperature.

Reliability of methodology

The dioxin formation from chlorophenol precursors involves two steps: the initial formation of predioxin from chlorophenol molecules, followed by the subsequent formation of dioxin through the ring closure mechanism. Figure 5 illustrates the

Fig. 5 Intrinsic reaction coordinates (IRCs) illustrating the ring closure mechanism of TCDD around TS_{R7} (a) and TS_{R11} . The flat line indicates the formation of stable bonds at the ends of the reaction coordinate



ring closure mechanism of TCDD which involves the progress of bond formation and bond dissociation in relation to the intrinsic reaction coordinate (IRC). As dioxin forms, several important chemical bonds are involved, including the breaking of O–H and C–Cl bonds and the formation of H–Cl and C–O bonds, contributing to the ring-closing process. During the reaction around TS_{R7} , the unbounded O atom attacks the chlorinated C atom at ortho position within predioxin molecule. This results in transitions of C–O bond formation from 2.83 to 1.39 Å, leading to the closure of the dioxin ring as expected from the mechanism. Simultaneously, the C–Cl bond in predioxin, initially bonded at 1.74 Å, stretches to 3.73 Å upon breaking, while the O–H bond, initially bonded at 0.97 Å, stretches to 2.13 Å upon breaking. During this process, an HCl molecule is eliminated, with a bond length of 1.29 Å, and before the reaction, both atoms are separated at a distance of 3.7 Å within the predioxin molecule. These changes align with the expected reaction mechanism. In a similar way, during the reaction around TS_{R11} , the negatively charged O atom attacks the chlorinated C atom at the ortho position within the predioxin-anion molecule, completing the dioxin ring. In this process, the C–Cl bond in predioxin anion (initially at 1.74 Å) breaks, releasing a chloride ion (Cl^-) at a distance of 3.19 Å from the initially bonded C atom. The flat line in Fig. 5 indicates the formation of a stable C–O bond (~1.37 Å) that closes the dioxin ring at the end of reactions R7 and R11, representing all proposed reaction pathways. This finding aligns with an ab-initio molecular dynamics study conducted by Farajian et al. [22], concluding that ring closure is only possible for two pathways (here reactions R7 and R11) out of their four proposed pathways for the ring closure mechanism.

To ensure the reliability of our computational approach, we first derived the stable molecular geometry of 2,3,7,8-tetrachlorodibenzo-p-dioxin (TCDD) using the B3LYP/6-311++G(d,p) level of theory. Subsequently, we compared these results with the existing experimental values [37]. Table 3 illustrates that the calculated bond lengths showed discrepancies from the experimental values ranging from –0.06% to +0.87% (except for 7.13% for the C–H bond). Similarly, the calculated bond angles showed differences of –0.66 to +0.43%. These marginal differences are consistent with those observed in prior theoretical calculations [21, 23]. Therefore, our findings confirm the reliability of computational method used for the molecular geometry as well as the proposed reaction mechanisms.

Conclusions

In this study, we have compared the formation mechanism of the highly toxic dioxin, 2,3,7,8-TCDD, from a common precursor, 2,4,5-trichlorophenol, through three different pathways: free-radical, direct condensation, and anionic

mechanisms. These calculations were studied under non-catalytic gas phase medium at 298.15 K and 1 atm. The quantum chemical calculations successfully found the transition state structures involved with each pathway and their corresponding energy barrier. Our findings indicate that the initial step of the mechanism (formation of predioxin) is clearly the rate determining step rather than the step corresponding to the formation of the tricyclic ring (dioxins), which aligns with the reported studies. This observation also aligns with an ab-initio molecular dynamics study that claim ring closure is only possible via intra-molecular condensation of predioxin (or predioxin anion). Also, our findings support the transition state theory indicating an increase in temperature is associated with the rise in Gibbs energy barrier particularly in the thermodynamically favorable pathway. This study addresses the issue of persistent organic pollutants (POPs) and their implications for sustainable development, particularly in environmental and ecological contexts. The results obtained can be used for designing reactors and incinerators with a suitable temperature range to control the emission of dioxins. This study will further elucidate the heterogeneous catalytic study to correlate the rate constant with the equilibrium constant using partition function approach.

Supplementary Information The online version contains supplementary material available at <https://doi.org/10.1007/s00894-024-05999-w>.

Acknowledgements The authors acknowledge the PARAM-ISHAN and PARAM-KAMRUPA supercomputing facility at IIT Guwahati for computational analyses. Additionally, R.H. is grateful to the Ministry of Education, Government of India, for Doctoral Fellowships.

Author contribution RH: Investigation, Data curation, Methodology, Validation, Formal analysis, Visualization, Writing – original draft, Writing – review & editing. Sk. MA: Conceptualization, Investigation, Software, Supervision, Methodology, Writing – review & editing. GP and TB: Supervision, Resources, Project administration, Writing – review & editing.

Data availability No datasets were generated or analysed during the current study.

Declarations

Competing interests The authors declare no competing interests.

References

1. Jasrotia R, Langer S, Dhar M (2021) Endocrine disrupting chemicals in aquatic ecosystem: an emerging threat to wildlife and human health. *Proc Zool Soc* 74(4):634–647. <https://doi.org/10.1007/s12595-021-00410-5>
2. Tue NM, Takahashi S, Subramanian A, Sakai S, Tanabe S (2013) Environmental contamination and human exposure to dioxin-related compounds in e-waste recycling sites of developing

- countries. *Environ Sci Process Impacts* 15(7):1326. <https://doi.org/10.1039/c3em00086a>
3. Karasek FW, Onuska FI (1982) Trace analysis of the dioxins. *Anal Chem* 54(2):309–324. <https://doi.org/10.1021/ac00239a002>
 4. Michalek JE, Tripathi RC (1999) Pharmacokinetics of TCDD in veterans of Operation Ranch Hand: 15-year follow-up. *J Toxicol Environ Heal - Part A*, 57 (6), 369–378. <https://doi.org/10.1080/009841099157584>
 5. Miniero R, De Felip E, Ferri F, Di Domenico A (2001) An overview of TCDD half-life in mammals and its correlation to body weight. *Chemosphere* 43(4–7):839–844. [https://doi.org/10.1016/S0045-6535\(00\)00442-2](https://doi.org/10.1016/S0045-6535(00)00442-2)
 6. Pavuk M, Michalek JE, Ketchum NS (2006) Prostate cancer in US Air Force veterans of the Vietnam war. *J Expo Sci Environ Epidemiol* 16(2):184–190. <https://doi.org/10.1038/sj.jea.7500448>
 7. Ying Y, Ma Y, Li X, Lin X (2021) Emission characteristics and formation pathways of PCDD/Fs from cocombustion of municipal solid waste in a large-scale coal-fired power plant. *Energy Fuels* 35(9):8221–8233. <https://doi.org/10.1021/acs.energyfuels.1c00714>
 8. Tuppurainen K, Asikainen A, Ruokojärvi P, Ruuskanen J (2003) Perspectives on the formation of polychlorinated dibenzo-p-dioxins and dibenzofurans during municipal solid waste (MSW) incineration and other combustion processes. *Acc Chem Res* 36(9):652–658. <https://doi.org/10.1021/ar020104+>
 9. Peng Y, Lu S, Li X, Yan J, Cen K (2020) Formation, measurement, and control of dioxins from the incineration of municipal solid wastes: recent advances and perspectives. *Energy Fuels* 34(11):13247–13267. <https://doi.org/10.1021/acs.energyfuels.0c02446>
 10. Lin F, Xiang L, Sun B, Li J, Yan B, He X, Liu G, Chen G (2021) Migration of chlorinated compounds on products quality and dioxins releasing during pyrolysis of oily sludge with high chlorine content. *Fuel* 306:121744. <https://doi.org/10.1016/j.fuel.2021.121744>
 11. Wang B, Fiedler H, Huang J, Deng S, Wang Y, Yu G (2016) A primary estimate of global PCDD/F release based on the quantity and quality of national economic and social activities. *Chemosphere* 151:303–309. <https://doi.org/10.1016/j.chemosphere.2016.02.085>
 12. Altarawneh M (2022) Temperature-dependent profiles of dioxin-like toxicants from combustion of brominated flame retardants. *J Hazard Mater* 422:126879. <https://doi.org/10.1016/j.jhazmat.2021.126879>
 13. Altwicker ER, Milligan MS (1993) Formation of dioxins: competing rates between chemically similar precursors and de novo reactions. *Chemosphere* 27(1–3):301–307. [https://doi.org/10.1016/0045-6535\(93\)90306-P](https://doi.org/10.1016/0045-6535(93)90306-P)
 14. McKay G (2002) Dioxin characterisation, formation and minimisation during municipal solid waste (MSW) incineration: review. *Chem Eng J* 86(3):343–368. [https://doi.org/10.1016/S1385-8947\(01\)00228-5](https://doi.org/10.1016/S1385-8947(01)00228-5)
 15. Stanmore BR (2004) The formation of dioxins in combustion systems. *Combust Flame* 136(3):398–427. <https://doi.org/10.1016/j.combustflame.2003.11.004>
 16. Mubeen I, Buekens A, Chen Z, Lu S, De YJ (2017) novo formation of dioxins from milled model fly ash. *Environ Sci Pollut Res* 24(23):19031–19043. <https://doi.org/10.1007/s11356-017-9528-x>
 17. Huang H, Buekens A (1995) On the mechanisms of dioxin formation in combustion processes. *Chemosphere* 31(9):4099–4117. [https://doi.org/10.1016/0045-6535\(95\)80011-9](https://doi.org/10.1016/0045-6535(95)80011-9)
 18. Dickson LC, Lenoir TD (1992) *Quantitative comparison of de novo and precursor formation of polychlorinated dibenzo-p-dioxins under simulated municipal solid waste incinerator postcombustion conditions*; 26.
 19. Altwicker ER (1996) Formation of PCDD/F in municipal solid waste incinerators: laboratory and modeling studies. *J Hazard Mater* 47(1–3):137–161. [https://doi.org/10.1016/0304-3894\(95\)00121-2](https://doi.org/10.1016/0304-3894(95)00121-2)
 20. Luijk R, Akkerman DM, Slot P, Olie K, Kapteijn F (1994) Mechanism of formation of polychlorinated dibenzo-p-dioxins and dibenzofurans in the catalyzed combustion of carbon. *Environ Sci Technol* 28(2):312–321. <https://doi.org/10.1021/es00051a019>
 21. Okamoto Y (1999) Formation pathways from 2,4,5-trichlorophenol (TCP) to polychlorinated dibenzo-p-dioxins (PCDDs): an ab initio study. *J Phys Chem A* 103(38):7686–7691. <https://doi.org/10.1021/jp991383u>
 22. Farajian AA, Mikami M, Ordejón P, Tanabe K (2001) Ring closure in dioxin formation process: an ab initio molecular dynamics study. *J Chem Phys* 115(14):6401–6405. <https://doi.org/10.1063/1.1402164>
 23. Suárez E, Suárez D, Menéndez MI, López R, Sordo TL (2006) Formation of trichlorinated dibenzo-p-dioxins from 2,4-dichlorophenol and 2,4,5-trichlorophenolate: a theoretical study. *ChemPhysChem* 7(11):2331–2338. <https://doi.org/10.1002/cphc.20060355>
 24. Frisch MJ, Trucks GW, Schlegel HB, Scuseria GE, Robb MA, Cheeseman JR, Scalmani G, Barone V, Petersson GA, Nakatsuji H, Li X, Caricato M, Marenich AV, Bloino J, Janesko BG, Gomperts R, Mennucci B, Hratch DJ Gaussian (2016) Inc., Wallingford CT
 25. Becke AD (1988) Density-functional exchange-energy approximation with correct asymptotic behavior. *Phys Rev A* 38(6):3098–3100. <https://doi.org/10.1103/PhysRevA.38.3098>
 26. Lee C, Yang W, Parr RG (1988) Development of the Colle-Salvetti correlation-energy formula into a functional of the electron density. *Phys Rev B* 37(2):785–789. <https://doi.org/10.1103/PhysRevB.37.785>
 27. McLean AD, Chandler GS (1980) Contracted Gaussian basis sets for molecular calculations. I. Second row atoms, Z=11–18. *J Chem Phys* 72 (10), 5639–5648. <https://doi.org/10.1063/1.438980>
 28. Dennington Roy, Keith Todd A, Millam JM (2016) GaussView, Version 6. Semichem Inc.: Shawnee Mission, KS
 29. Gonzalez C, Bernhard Schlegel H (1989) An improved algorithm for reaction path following. *J Chem Phys* 90(4):2154–2161. <https://doi.org/10.1063/1.456010>
 30. Gonzalez C, Schlegel HB (1990) Reaction path following in mass-weighted internal coordinates. *J Phys Chem* 94(14):5523–5527. <https://doi.org/10.1021/j100377a021>
 31. Altarawneh M, Dlugogorski BZ, Kennedy EM, Mackie JC (2009) Mechanisms for formation, chlorination, dechlorination and destruction of polychlorinated dibenzo-p-dioxins and dibenzofurans (PCDD/Fs). *Prog Energy Combust Sci* 35(3):245–274. <https://doi.org/10.1016/j.pecs.2008.12.001>
 32. Baker J, Scheiner A, Andzelm J (1993) Spin contamination in density functional theory. *Chem Phys Lett* 216(3–6):380–388. [https://doi.org/10.1016/0009-2614\(93\)90113-F](https://doi.org/10.1016/0009-2614(93)90113-F)
 33. Truhlar DG, Garrett BC, Klippenstein SJ (1996) Current status of transition-state theory. *J Phys Chem* 100(31):12771–12800. <https://doi.org/10.1021/jp953748q>
 34. Gibbs JW, Tyndall J (1876) On the equilibrium of heterogeneous substances : first [-second] part. *Equilib. Heterog. Subst. first [-second] part* 108–248. <https://doi.org/10.5479/sil.421748.39088007099781>
 35. Laury ML, Carlson MJ, Wilson AK (2012) Vibrational frequency scale factors for density functional theory and the polarization

- consistent basis sets. *J Comput Chem* 33(30):2380–2387. <https://doi.org/10.1002/jcc.23073>
36. te Velde G, Bickelhaupt FM, Baerends EJ, Fonseca Guerra C, van Gisbergen SJA, Snijders JG, Ziegler T (2001) Chemistry with ADF. *J Comput Chem* 22(9):931–967. <https://doi.org/10.1002/jcc.1056>
37. Boer FP, Neuman MA, Van Remoortere FP (1973) X-ray diffraction studies of chlorinated dibenzo-p-dioxins. In *Advances in Chemistry Series*; 120, pp 14–25. <https://doi.org/10.1021/ba-1973-0120.ch003>

Publisher's Note Springer Nature remains neutral with regard to jurisdictional claims in published maps and institutional affiliations.

Springer Nature or its licensor (e.g. a society or other partner) holds exclusive rights to this article under a publishing agreement with the author(s) or other rightsholder(s); author self-archiving of the accepted manuscript version of this article is solely governed by the terms of such publishing agreement and applicable law.